

Performance of RC moment frames with fixed and hinged supports under near-fault ground motions

Mohammad Hossain Mohammadi^a, Ali Massumi^{*} and Afshin Meshkat-Dini^b

Department of Civil Engineering, Faculty of Engineering, Kharazmi University, Tehran, 15719-14911, Iran

(Received January 17, 2017, Revised May 29, 2017, Accepted June 20, 2017)

Abstract. The focus of this paper is the study on the seismic performance of RC buildings with two different connections at the base level under near-fault earthquakes. It is well-known that the impulsive nature of the near-fault ground motions causes severe damages to framed buildings especially at base connections. In the scope of this study, two types of 3-dimensional RC Moment Frames with Fixed Support (MFFS) and Hinged Support (MFHS) containing 5 and 10 stories are assessed under an ensemble of 11 strong ground motions by implementing nonlinear response history analysis. The most vulnerable locations of MFFS, are the connections of corner columns to foundation especially under strong earthquakes. On the other hand, using beams at the base level as well as hinged base connections in MFHS buildings, prevents damages of corner columns and achieves more ductile behavior. Results denote that the MFHS including Base Level Beams (BLB) significantly shows better behavior compared with MFFS, particularly under pulse-type records. Additionally, the first story beams and also interior components undergo more actions. Role of the BLBs are similar to fuses decreasing the flexural moments of the corner columns. The BLBs can be constructed as replaceable members which provide the reparability of structures.

Keywords: seismic performance; RC moment frame; hinged base; base level beam; near-fault ground motions

1. Introduction

Besides strength, ductility was considered as another essential property for structures to survive strong earthquakes in the 1950s. Due to the lack of appropriate ductility, many reinforced concrete frames have experienced failures in the kind of local mechanism under earthquakes. Ductility makes the strength of the whole structure can be better developed (Qu *et al.* 2012). Behavior factor or force reduction factor significantly associates with ductility of structure and makes it possible to design for only a fraction of the earthquake-induced forces. Providing desirable ductility, results in dissipating input earthquake energy through hysteretic behavior (Massumi 2004, Tasnimi and Massumi 2007). The strong column-weak beam criterion, which was proposed and discussed extensively by Paulay and Priestley (1992), is the most important rule in seismic design of moment frames. On the other hand, strong near-fault earthquakes with pulse-type nature have shown severe damages. Occurrence of catastrophic earthquakes such as Landers 1992, Northridge 1994, Kobe 1995 and Chi-Chi 1999 in decade 90, led extensive researches toward near-fault effects on structural designing (Stewart *et al.* 2001). Propagation of fault rupture with the velocity close

to the shear wave velocity toward a site generates forward-directivity effects and accumulation of seismic radiations results in forming a long-period and high-amplitude pulse in the beginning of the velocity history. Due to the inclination of shear waves' accumulation toward the normal direction of rupture, the fault-normal components are stronger than the fault-parallel ones (Alavi and Krawinkler 2001). In 1975, the pulses of near-fault records have been distinguished for the first time (Bolt 1975). Seismic demands are widely concerned with the ratio of the velocity pulse period to the fundamental period ($T_{\text{pulse}}/T_{\text{structure}}$) and the ratio of the PGA to the lateral stiffness. Generally, high deflections in lower stories enhance the axial forces of columns and also P- Δ effects in lower stories (Anderson and Bertero 1987).

Champion and Liel (2012) comprehensively researched on the ratio of the pulse period to the fundamental period of structure ($T_{\text{pulse}}/T_{\text{structure}}$) and have declared that structures which were designed elastic, experienced the highest demand when $T_{\text{pulse}}/T_{\text{structure}}$ equaled 1. Whereas, ductile structures underwent the highest demand in $T_{\text{pulse}}/T_{\text{structure}}$ close to 2, due to the elongation of period before collapse. Their study also demonstrated the importance of considering directivity effects in seismic hazard analysis and simulation of structural response.

Fling step in the parallel direction of faulting appears like a static displacement and typically excites the first mode of structural vibration (Kalkan and Kunnath 2006). Alavi and Krawinkler (2001) recognized the high seismic demands of structures in the direction of the fault-normal component and also claimed that the spectral analysis yielded inappropriate results. The excitation of higher modes in high-rise buildings, due to wave travelling effect,

*Corresponding author, Professor

E-mail: massumi@khu.ac.ir

^aM.Sc. student

E-mail: std_h.mohammadi@khu.ac.ir

^bAssistant Professor

E-mail: meshkat@khu.ac.ir

causes to premature yield. Consequently, the upper stories quickly reach to their shear capacity. They proposed using hinged walls to strengthen frame structures subjected to near-fault ground motions. It was also found that employing hinged walls was effective in decreasing the story drift demands and producing a more uniform distribution of story drifts over the height of the building. Moreover, the shear and moment demands for a hinged wall were much lower than those for a fixed-base wall (Alavi and Krawinkler 2004). Massumi *et al.* (2015) evaluated the seismic response of RC frame structures strengthened by reinforced masonry infill panels. They concluded that, the use of infill panels in low-rise RC frame structures was an effective way of improving seismic performance during earthquakes, however, their results related to far-fault earthquakes. Zhai *et al.* (2016) investigated on the seismic response of nonstructural components considering the pulse-type motions and proposed suitable formulation of amplification factors for design of nonstructural components.

Different procedures for enhancing the seismic performance through base isolation (Ponzo *et al.* 2012, Mazza 2015a, 2017) or energy dissipation (Sorace and Terenzi 2014, Mazza 2015b) systems were performed to mitigate near-fault effects.

Nowadays, the reparability is the most essential property of buildings experienced strong earthquakes. Reparability denotes preventing major damages to columns and foundations. Columns in MFFS buildings are susceptible to severe structural damage such as premature formation of plastic hinges at their feet and soft-story failure. Columns and footings must be protected due to the difficulties associated with their repairs and replacements (Grigorian and Grigorian 2015).

This paper studies on the influence of hinged base connections and also the function of BLBs in decreasing damages of RC frame structures under strong near-fault earthquakes. Two types of similar MFFS and MFHS buildings with 5 and 10 stories are assessed on the basis of ASCE/SEI 41-13. Results reveal the superiority of the MFHS against the MFFS, especially for 10-story building, because of better mobilization of ductility and avoidance of corner column collapse.

2. Structural specifications and response history analyses

2.1 Structural models

Two types of 3-dimensional regular reinforced concrete buildings including 5 and 10 stories erected on soil type 2 ($v_s=375-750$ m/s) are designed according to ACI 2014 code. The seismic loading and analysis are based on Iranian seismic code, IS 2800-14 (Standard No. 2800-4th Edition). IS 2800 is considerably similar to ASCE 7 (ASCE/SEI). The compressive strength and Young modulus of concrete are assumed 25 MPa and 26 GPa, respectively. Yield strength and Young modulus of reinforcement steel are also assumed 400 MPa and 200 GPa, respectively. Plan and elevations of the buildings are shown in Fig. 1. Dimensions and reinforcement of the MFFS buildings are reported in Table 1 and Table 2. It is worth pointing out here that the dimensions and reinforcement of the MFHS buildings are obtained identical to the MFFS buildings according to design process. Despite the BLBs require smaller size of reinforcement, their reinforcement are selected equal to the first story beams in order to reach similar dynamic properties. If the dynamic properties of the MFFS and the MFHS are similar, the evaluation and comparison of performances will be reasonable. For the latter purpose, the reinforcements of BLBs are chosen equal to the first story beams reinforcement. The modal analysis results of both types of buildings (Table 3) and also the capacity curves of them are approximately equivalent. For instance, the capacity curves with pattern of the first mode are illustrated in Fig. 2. Dead and live loads are considered 5.5 kN/m² and 2 kN/m² for typical stories and 6 kN/m² and 1.5 kN/m² for roof, respectively. Equivalent dead load of circumferential walls and interior partition walls are considered 2 kN/m² and 1.5 kN/m². Seismic mass includes 100% of dead load and 20% of live load, for residential buildings. Modal analysis results are provided in Table 3. In order to design of the buildings, spectral analysis is implemented, using Iranian design spectrum existing in IS 2800-14. Due to the destructive manner of near-fault earthquakes, the strong column and weak beam rule is absolutely observed in seismic design.

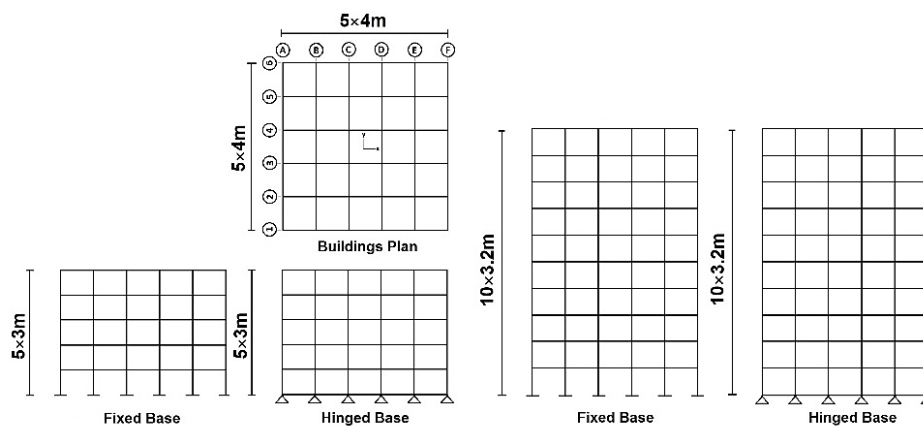


Fig. 1 Plan and elevations of studied buildings

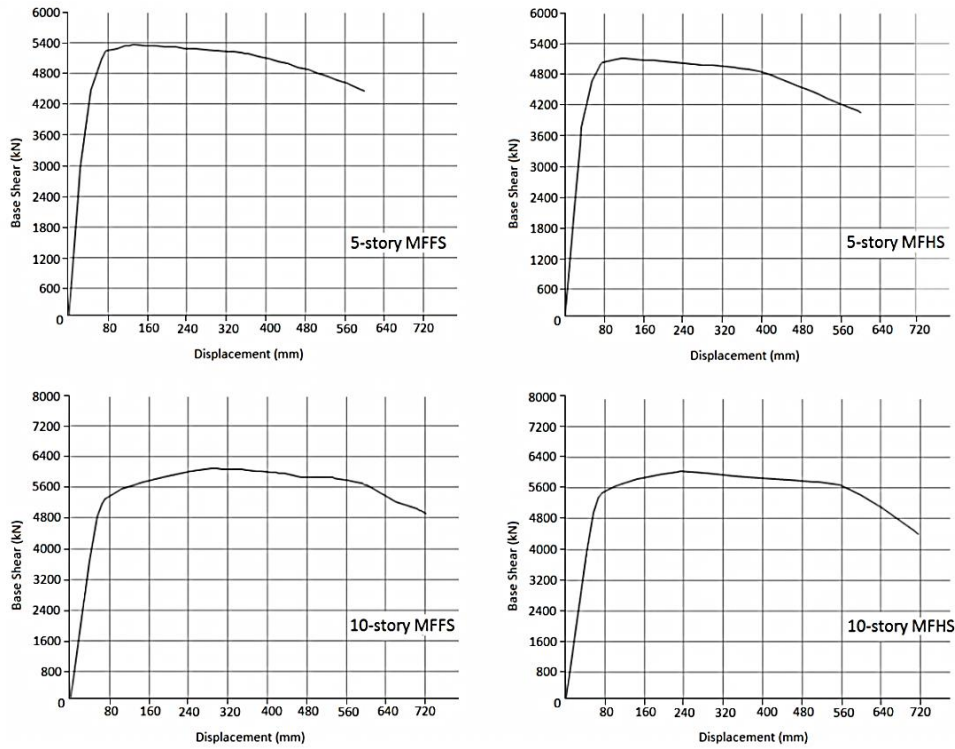


Fig. 2 Capacity curve of the MFSS and the MFHS (first mode pattern of pushover)

Table 1 Structural details of the 5-story buildings

Story	Beams		Columns	
	b _{xh} (No.-Bar Size)	Av/S	b _{xh} (No.-Bar Size)	Av/S
1	45×45 (4-20d)	0.1	50×50 (20-20d)	0.157
2	45×45 (4-20d)	0.1	50×50 (20-20d)	0.157
3	40×40 (4-20d)	0.1	45×45 (16-18d)	0.157
4	40×40 (4-18d)	0.1	45×45 (16-18d)	0.157
5	40×40 (4-18d)	0.1	45×45 (12-18d)	0.157

Dimensions are in centimeter

Table 2 Structural details of the 10-story buildings

Story	Beams		Columns	
	b _{xh} (No.-Bar Size)	Av/S	b _{xh} (No.-Bar Size)	Av/S
1	50×50 (4-20d)	0.157	55×55 (20-20d)	0.157
2	50×50 (5-20d)	0.157	55×55 (20-20d)	0.157
3	45×45 (5-20d)	0.157	50×50 (16-20d)	0.157
4	45×45 (5-20d)	0.157	50×50 (16-20d)	0.157
5	45×45 (5-20d)	0.157	50×50 (16-20d)	0.157
6	45×45 (6-18d)	0.157	50×50 (16-20d)	0.157
7	40×40 (5-18d)	0.157	50×50 (16-18d)	0.157
8	40×40 (5-18d)	0.157	50×50 (16-18d)	0.157
9	40×40 (5-18d)	0.157	50×50 (16-18d)	0.157
10	40×40 (5-18d)	0.157	50×50 (16-18d)	0.157

Dimensions are in centimeter

Table 3 Modal analysis results of the first nine modes

Mode	ID	Period (s)			
		5-MFSS	5-MFHS	10- MFSS	10- MFHS
1	T1X	0.66	0.70	1.07	1.08
2	T1Y	0.66	0.70	1.07	1.08
3	T1θ	0.60	0.64	0.97	0.97
4	T2X	0.21	0.23	0.37	0.38
5	T2Y	0.21	0.23	0.37	0.38
6	T2θ	0.19	0.21	0.34	0.34
7	T3X	0.11	0.12	0.21	0.22
8	T3Y	0.11	0.12	0.21	0.22
9	T3θ	0.10	0.11	0.19	0.20

2.2 Ground motions selected in this study

11 ground motions, from earthquakes with moment magnitude greater than 6.5, are selected from PEER ground motion database. Table 4 provides the characteristics of the selected ensemble. Some of the velocity pulses are shown in Fig. 3. Fault-parallel or longitudinal component (LN) and fault-normal or transversal component (TR) are applied in the structural direction of X and Y, respectively. The ELC earthquake with a hypocentral distance of 12.2 km, contains no directivity effects and is considered as a strong far-fault earthquake. Other earthquakes are near-fault with forward-directivity effects, except JOS, involving backward-directivity effects. Intensity-based scaling of the ground motions are used to match the earthquakes spectra to Iranian design spectrum in the period range of 0.2T to 1.5T, where T is the first mode translational period.

Table 4 Characteristics of selected ensemble and abbreviations

No.	Event	Station	v_s (m/s)	R_{rup} (km)	Component ID	SD* (s)	T_{pulse}^* (s)
1	Imperial valley-02	El Centro Array #9	213.44	6.09	ELC-LN	23.63	----
					ELC-TR	23.84	----
2	Manjil, Iran	Abbar	723.95	12.5	ABR-LN	10.76	----
					ABR-TR	20.02	2.00
3	Northridge -01 1994	LA-SepulvedaV A Hospital	380.06	8.44	SPV-LN	8.26	0.60
					SPV-TR	7.86	1.00
4	Northridge -01 1994	Newhall-WPico Canyon Rd.	285.93	5.48	WPI-LN	10.91	0.80
					WPI-TR	6.97	2.00
5	Erzican, Turkey	Erzincan	352.05	4.38	ERZ-LN	11.80	1.00
					ERZ-TR	15.31	3.00
6	Bam, Iran	Bam	487.40	1.70	BAM-LN	8.70	1.60
					BAM-TR	7.77	1.50
7	Tabas, Iran	Tabas	766.70	2.05	TAB-LN	16.36	0.75
					TAB-TR	16.10	6.20
8	Imperial valley-06	El Centro Array #6	203.22	1.35	E06-LN	11.42	2.00
					E06-TR	8.24	3.70
9	Imperial valley-06	El Centro Array #7	210.51	0.56	E07-LN	6.75	1.50
					E07-TR	4.80	3.00
10	Landers	Lucern	1369.0	2.19	LCN-LN	13.78	----
					LCN-TR	13.50	4.80
11	Landers	Joshua Tree	379.32	11.0	JOS-LN	26.94	----
					JOS-TR	25.98	----

* SD and T_{pulse} denote significant duration and velocity pulse period, respectively

2.3 Modeling of components and response history analyses

For the assessment of RC buildings by applying nonlinear analysis, SAP2000 version 18.1.1 software is employed. The provisions and instructions of ASCE/SEI 41-13 (Seismic Evaluation and Retrofit of Existing Buildings) are used for modeling nonlinear behavior of components, considering concentrated plastic hinge. According to ASCE 41-13, customary behavior curve of a deformation-controlled component is similar to Fig. 4.

The following conditions are considered in seismic analyses and assessment:

1. Deformation-controlled hinges are located at the distances equal to the half-height of members from end rigid zones and they also follow Takeda hysteresis model (Takeda *et al.* 1970).
2. Based on the axial force value, columns may behave either in ductile manner or brittle manner, therefore, this issue is considered according to ASCE 41-13 criteria in modelling.
3. Nonlinear analyses are implemented by using HHT direct integration method (Hilber *et al.* 1977), considering damping ratio of 5%.
4. Connections and diaphragms are rigid and P- Δ effect is considered in the analysis.
5. Fault-parallel and fault normal components of records are applied in the X and Y structural directions, respectively.

It should be noted that the ratio $\frac{P}{A_g f_c}$ dominates the behavior of columns as well as shear reinforcement and should be cared in the nonlinear modelling. As an instance,

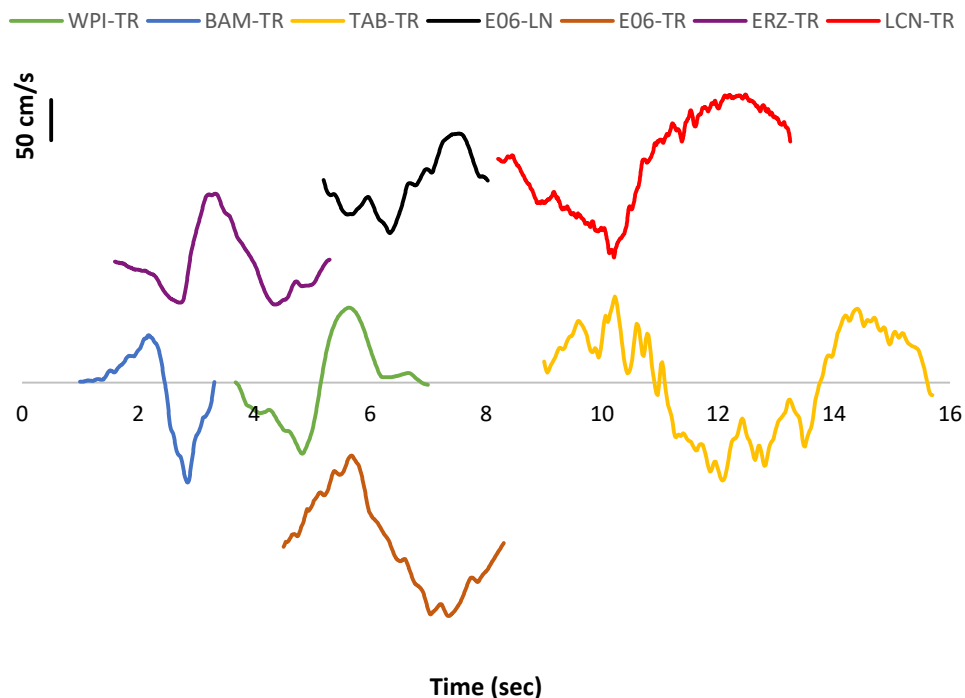


Fig. 3 Some of the existing pulses in the velocity history of records

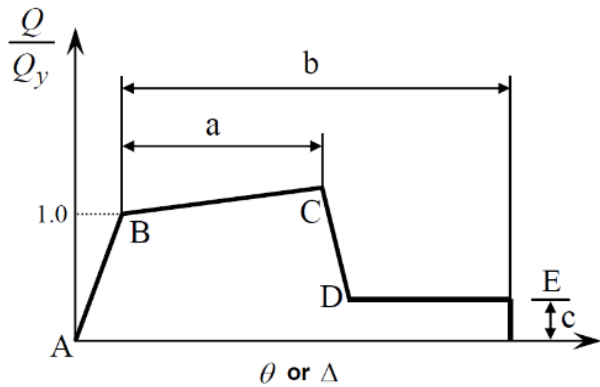


Fig. 4 Generalized force-deformation relation for RC ductile components (after ASCE/SEI 41-13)

Table 5 Base shears (kN) and performance levels of the 5-story buildings

Earthquake	MFFS			MFHS		
	V-X	V-Y	PL*	V-X	V-Y	PL*
ELC	5442.50	5978.20	IO	5093.50	5921.00	IO
ABR	6088.90	6378.60	IO	5890.20	5637.50	IO
SPV	6701.10	7248.40	CP	5740.60	6999.40	CP
WPI	7830.70	12469.00	CP	6805.70	8030.20	CP
ERZ	5842.10	7154.90	LS	5593.10	6409.90	LS
BAM	6924.90	8061.50	LS	6532.10	7374.30	LS
TAB	6461.20	7130.60	CP	6259.90	6684.30	CP
E06	6774.60	7710.30	LS	5663.90	6505.50	LS
E07	7510.60	7301.50	LS	5781.40	6151.10	LS
LCN	6125.10	10116.90	CP	5800.80	7414.90	CP
JOS	6729.80	8502.20	CP	5867.30	6418.20	CP
Average	6584.70	8004.70	-----	5540.70	6629.40	-----

*PL: Performance Level

if the latter ratio does not exceed 10 percent, the column will behave in flexural manner like a beam. Table 10-8 of ASCE 41-13 presents the conditions and the parameters for nonlinear modeling of RC columns.

3. Results

3.1 Base shear demand

Based on the results of the spectral analysis, both types of the 5- and 10-story buildings have been designed for the base shears of 3225.1 and 4621.5 kN, respectively. It is appropriate to implement nonlinear response history analysis for assessing the relatively accurate manners of structures. As reported in Table 5 and Table 6, both types of buildings collapsed under majority of near-fault ground motions. Base shear demands of the MFHS are not varied considerably against the MFFS especially for 5-story buildings, while the damage pattern of the MFHS buildings are significantly varied.

Table 6 Base shears (kN) and performance levels of the 10-story buildings

Earthquake	MFFS			MFHS		
	V-X	V-Y	PL*	V-X	V-Y	PL*
ELC	7483.80	7396.90	IO	7519.40	7713.60	IO
ABR	8156.30	9358.60	CP	8165.60	9386.00	LS
SPV	7012.50	10522.90	LS	8194.60	10111.10	LS
WPI	9113.40	9182.70	CP	8798.80	9708.30	CP
ERZ	6400.80	8805.40	CP	6993.70	8474.60	CP
BAM	4486.60	8971.80	CP	8140.90	9203.10	CP
TAB	7079.50	8976.90	CP	8773.70	9520.60	CP
E06	8849.50	9328.70	CP	8167.00	9055.40	CP
E07	8034.30	8780.60	CP	7880.40	8859.10	LS
LCN	7783.50	11468.30	CP	7295.50	10166.50	CP
JOS	6733.30	8079.30	IO	6982.60	7692.40	IO
Average	7375.80	9170.20	-----	7901.10	9081.00	-----

*PL: Performance Level

Another observatory denotes the improvement of performance levels of the 10-story MFHS buildings due to the desirable utilization of ductility before collapse. The damage patterns of the buildings will be discussed comprehensively in the next section.

3.2 Inter-story drift ratio demand and damage pattern

Recent researches related to the forward-directivity effects on stories displacement and vulnerability of structures, indicate the significant influence of $T_{pulse}/T_{structure}$. The larger $T_{pulse}/T_{structure}$, the higher inter-story drift ratio especially in lower stories (Sehhati *et al.* 2011). Further, a study on the correlation between intensity parameters of pulse-type motions and damage of low-rise RC frames demonstrates that, velocity spectrum intensity (VSI) provides the best correlation with the damage of structures in terms of either maximum inter-story drift or damage index (Van Cao and Ronagh 2014).

The inter-story drift ratios of the MFFS and the MFHS buildings are shown in Figs. 5-12. It is seen that the drift ratios of the Y-direction are larger than the X-direction in two types of buildings, since the TR components of near-fault earthquakes are stronger than the LN ones. Moreover, the inter-story drift ratios of MFHS buildings are increased in lower stories compared with the inter-story drift ratios of MFFS buildings. It is important to point out that, earthquakes such as TAB, E07 and ABR demonstrate small values of the inter-story drift ratios for the 10-story MFFS building, because of the abrupt collapses of the first story corner columns. On the other hand, the corresponding values for the MFHS building are enhanced, because of the changes in damage patterns. As a result of this study, the first story columns of MFFS, particularly corner columns, are the most vulnerable members under strong near-fault ground motions. While, for MFHS buildings, the BLBs and the first story beams play significant role and they function

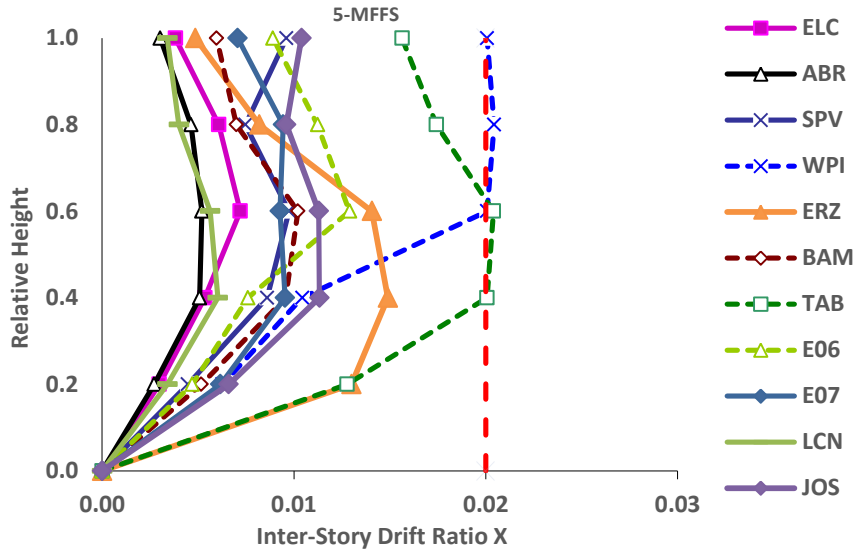


Fig. 5 Inter-story drift ratios of the 5-story MFSS building (X-Direction)

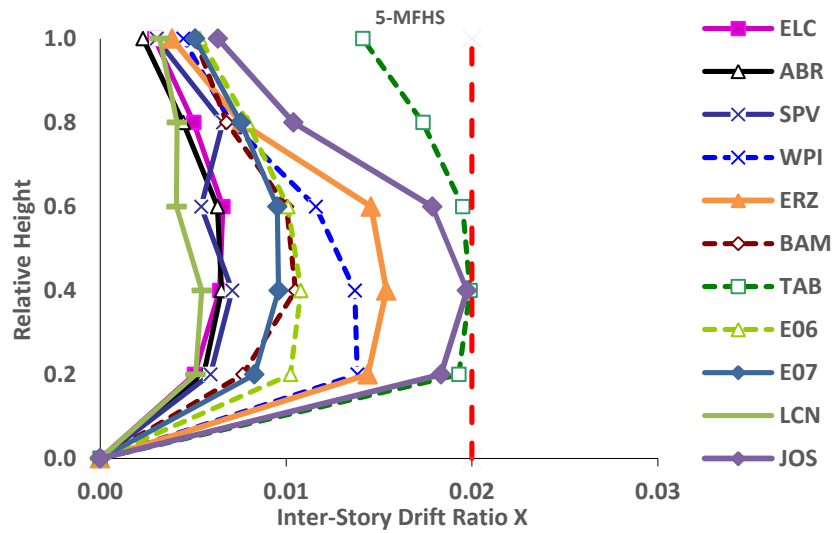


Fig. 6 Inter-story drift ratios of the 5-story MFHS building (X-Direction)

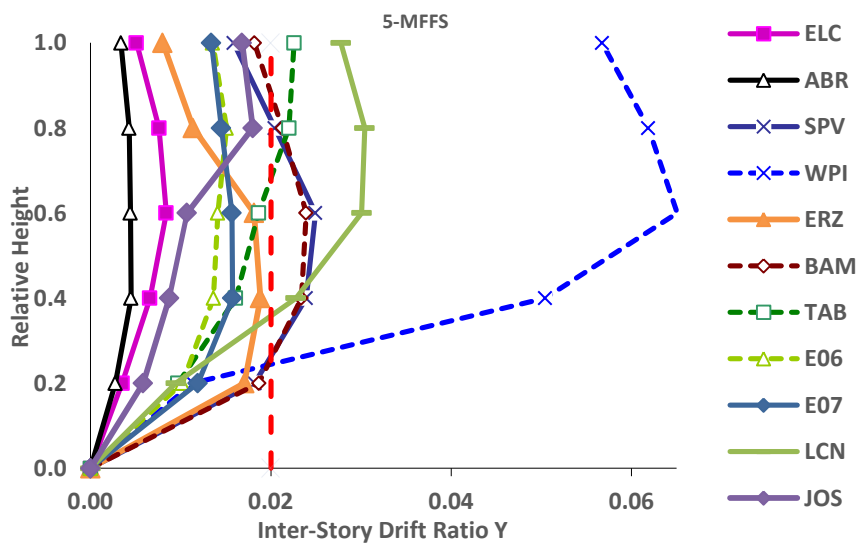


Fig. 7 Inter-story drift ratios of the 5-story MFSS building (Y-Direction)

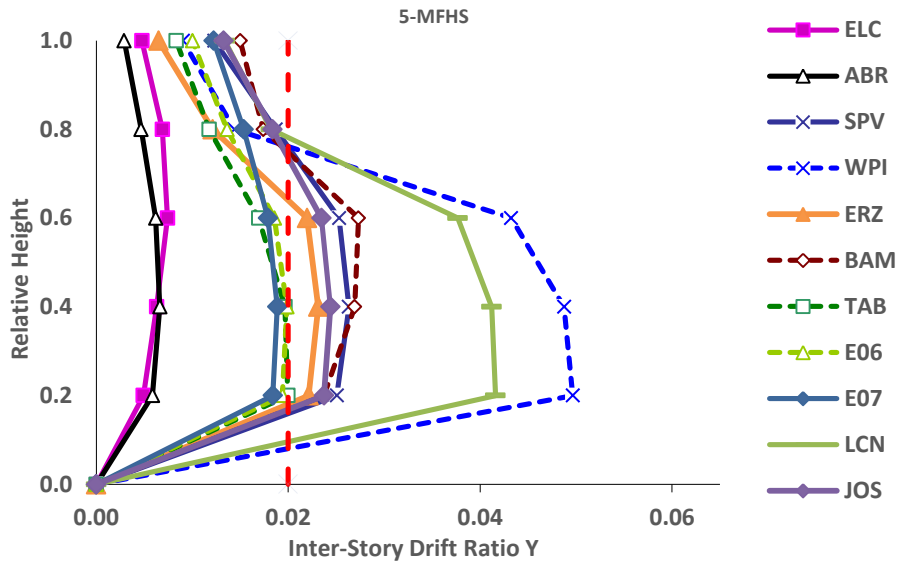


Fig. 8 Inter-Story drift ratios of the 5-story MFHS building (Y-Direction)

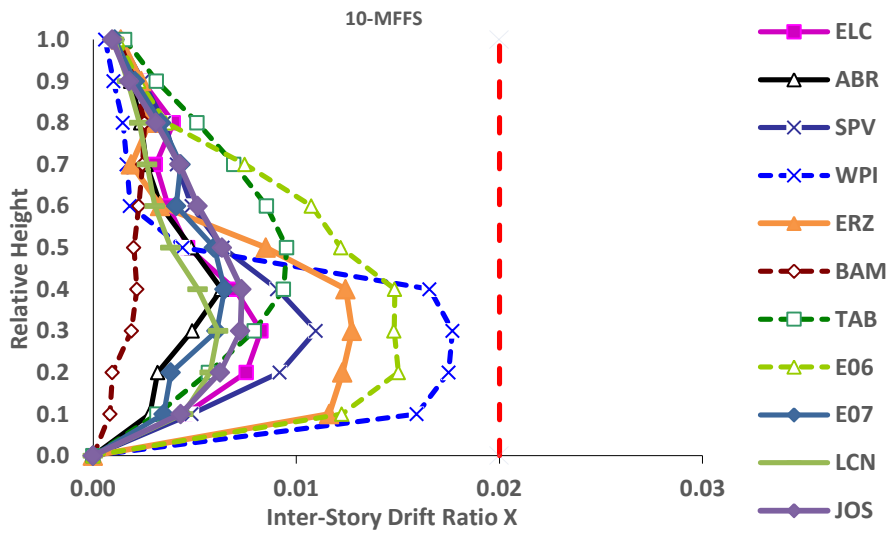


Fig. 9 Inter-story drift ratios of the 10-story MFHS building (X-Direction)

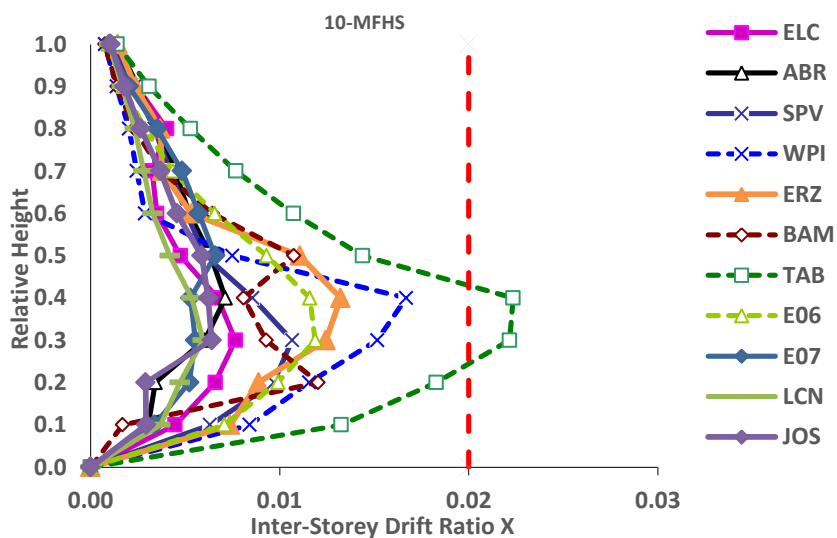


Fig. 10 Inter-story drift ratios of the 10-story MFHS building (X-Direction)

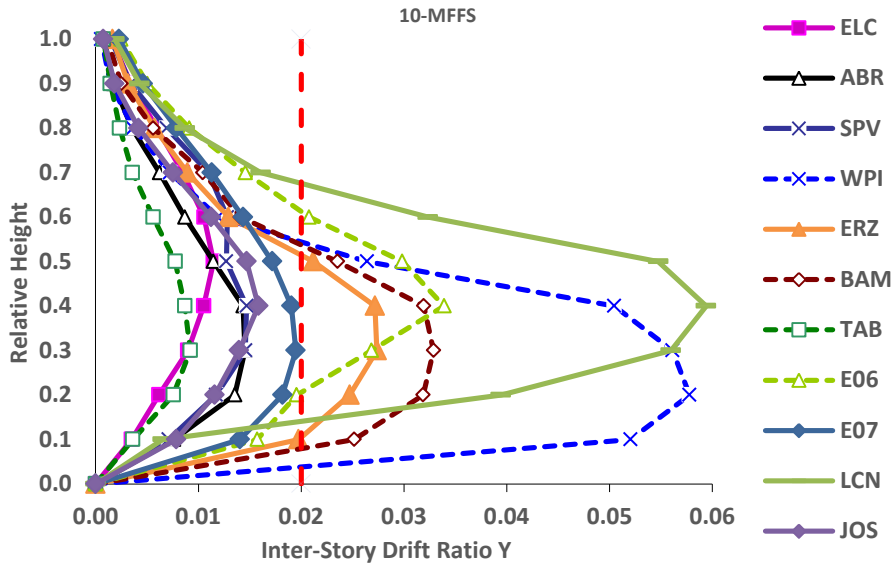


Fig. 11 Inter-story drift ratios of the 10-story MFFS building (Y-Direction)

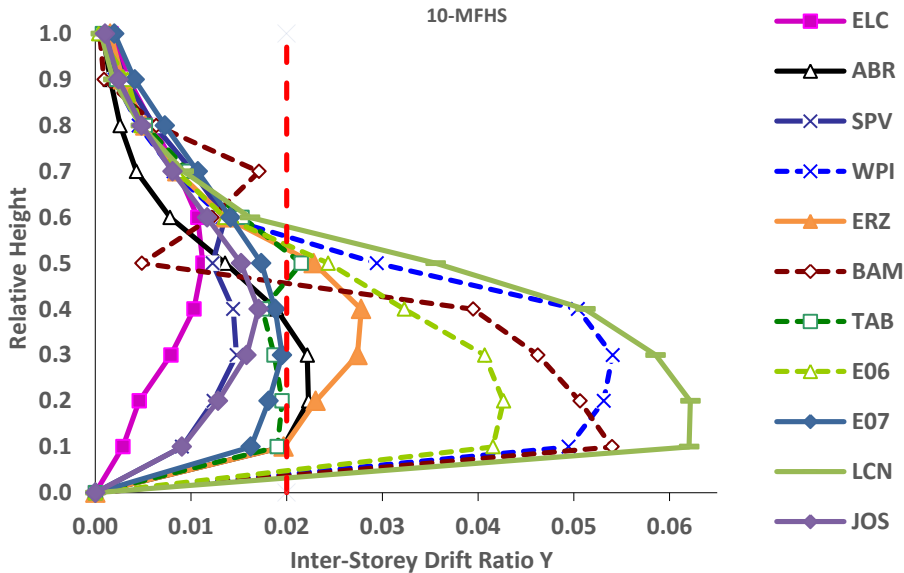


Fig. 12 Inter-story drift ratios of the 10-story MFHS building (Y-Direction)

Table 7 Pattern of damage and collapse time of the 5-story MFFS building

Record ID	Damage Pattern of 5-story MFFS building
ELC	No structural damage occurred.
ABR	No structural damage occurred.
SPV	2nd story beams of Y-direction reached CP level at the end of the velocity pulse (t=3.9 s).
WPI	2nd to 5th story beams reached CP level nearly at the end of the velocity pulse (t=5.8 s).
ERZ	1st and 2nd story beams and 1st story columns reached LS level.
BAM	All beams of Y-direction and 1st story columns reached LS level.
TAB	Abruptly, one of the 1st story corner columns reached CP level at 1st peak of the pulse (t=9.6 s).
E06	All beams of Y-direction and 1st story columns reached LS level.
E07	All beams of Y-direction and 1st story columns reached LS level.
LCN	Abruptly, one of the 1st story corner columns reached CP level after the 1st peak of the pulse (t=10.6 s).
JOS	Abruptly, one of the 1st story corner columns reached CP level at t=9.1 s, due to dynamic resonance.

Table 8 Pattern of damage and collapse time of the 5-story MFHS building

Record ID	Damage Pattern of 5-story MFHS building
ELC	No structural damage occurred.
ABR	No structural damage occurred.
SPV	1st and 2nd story beams of Y-direction reached CP level at the end of the velocity pulse (t=4.2 s).
WPI	Base to 2nd story beams reached CP level nearly at the end of the velocity pulse (t=5.8 s).
ERZ	Base to 2nd story beams and 3rd story columns reached LS level.
BAM	All beams of Y-direction and 1st story columns reached LS level.
TAB	All beams reached LS, then a side column of 4th story reached CP nearly at the end of the pulse (t=14.3 s).
E06	All beams of Y-direction reached LS level.
E07	All beams of Y-direction reached LS level.
LCN	Base to 2nd story beams reached CP level nearly at the half of the velocity pulse (t=11.2 s).
JOS	All beams reached LS, then a side column of 4th story reached CP at t=26.2 s, due to dynamic resonance.

Table 9 Pattern of damage and collapse time of the 10-story MFFS building

Record ID	Damage Pattern of 10-story MFFS building
ELC	No structural damage occurred.
ABR	Abruptly, one of the 1st story corner columns reached CP level at end of the velocity pulse (t=11.9 s).
SPV	2nd to 6th story beams of Y-direction reached LS level.
WPI	1st to 3rd story beams reached CP level at the half of the velocity pulse (t=5.2 s).
ERZ	1st to 3rd story beams and a corner column of 1st story reached CP level at the peak of the pulse (t=3.4 s).
BAM	1st to 4th story beams reached CP level at the same time with the end of the velocity pulse (t=3.3 s).
TAB	Abruptly, one of the 1st story corner columns reached CP level after the 1st peak of the pulse (t=10.9 s).
E06	2nd to 5th story beams of Y-direction reached CP level nearly after the half of velocity pulse (t=7 s).
E07	Abruptly, one of the 1st story corner columns reached CP level after the 1st peak of the velocity pulse (t=6.2 s).
LCN	Three columns of the first story reached CP level at t=10.8 s after the 1st peak of the velocity pulse.
JOS	No structural damage occurred.

Table 10 Pattern of damage and collapse time of the 10-story MFHS building

Record ID	Damage Pattern of 10-story MFHS building
ELC	No structural damage occurred.
ABR	Base to 4th story beams of Y-direction either reached or passed LS level.
SPV	1st to 5th story beams of Y-direction and 2nd story beams of X-direction reached LS level.
WPI	Base to 4th story beams of Y-direction reached CP level nearly at the end of the velocity pulse (t=6 s).
ERZ	2nd to 4th story beams of Y-direction reached CP level nearly at the end of the velocity pulse (t=4.5 s).
BAM	Base to 4th story beams of Y-direction reached CP level at t=3.6 s after the end of the velocity pulse.
TAB	4th story beams of Y-direction reached CP level nearly at the end of the velocity pulse (t=14.9 s).
E06	Base to 4th story beams of Y-direction reached CP level at the 2nd peak of the velocity pulse (t=7.3 s).
E07	Base to 6th story beams of Y-direction reached LS level.
LCN	Base to 4th story beams of Y-direction reached CP level at the 2nd peak of the velocity pulse (t=11.6 s).
JOS	No structural damage occurred.

like fuse members to eliminate the threat of corner columns collapses. For better assessment of structural manner, qualitative patterns of damages and times of collapses are summarized in Tables 7-10. Figs. 13-16 illustrate some instances of improved performances and collapse times of the MFHS against the MFFS.

According to ASCE 41-13 and ASCE 7, members'

plastic hinge rotation and maximum nonlinear inter-story drift ratio are known as current seismic performance indicators, associated with structural components (local scale) and whole structure (global scale), respectively.

As presented in Figs. 13-16, the improvements of seismic performance are observed especially for taller building. Due to the nature of near-fault records, providing

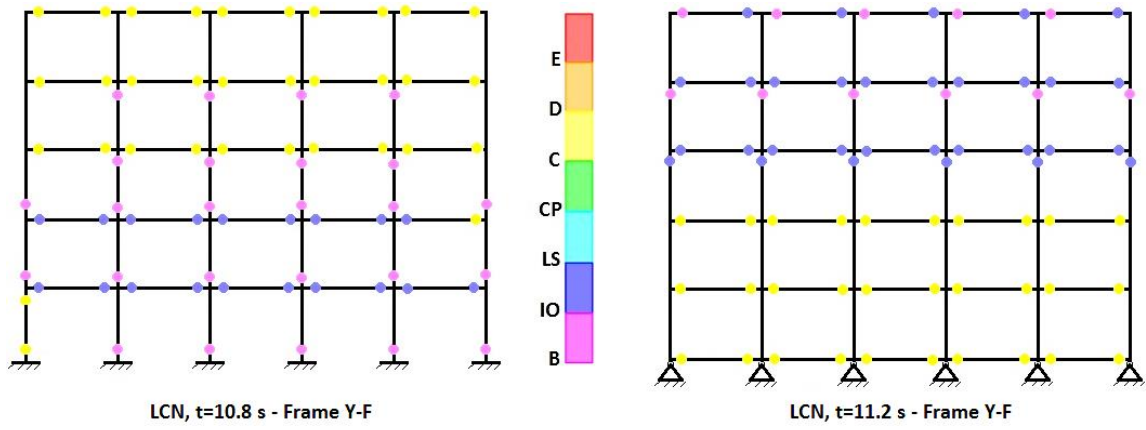


Fig. 13 Seismic performance levels of the 5-story buildings under LCN

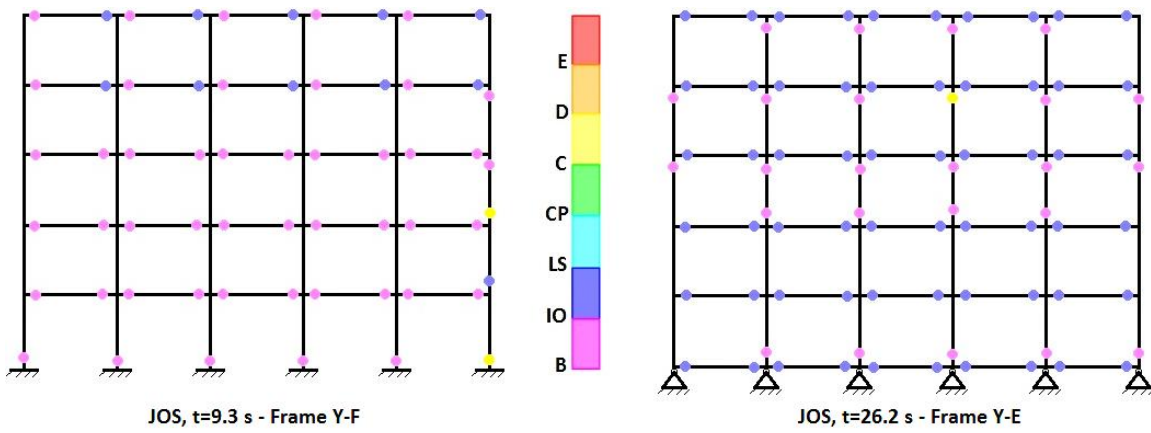


Fig. 14 Seismic performance levels of the 5-story buildings under JOS

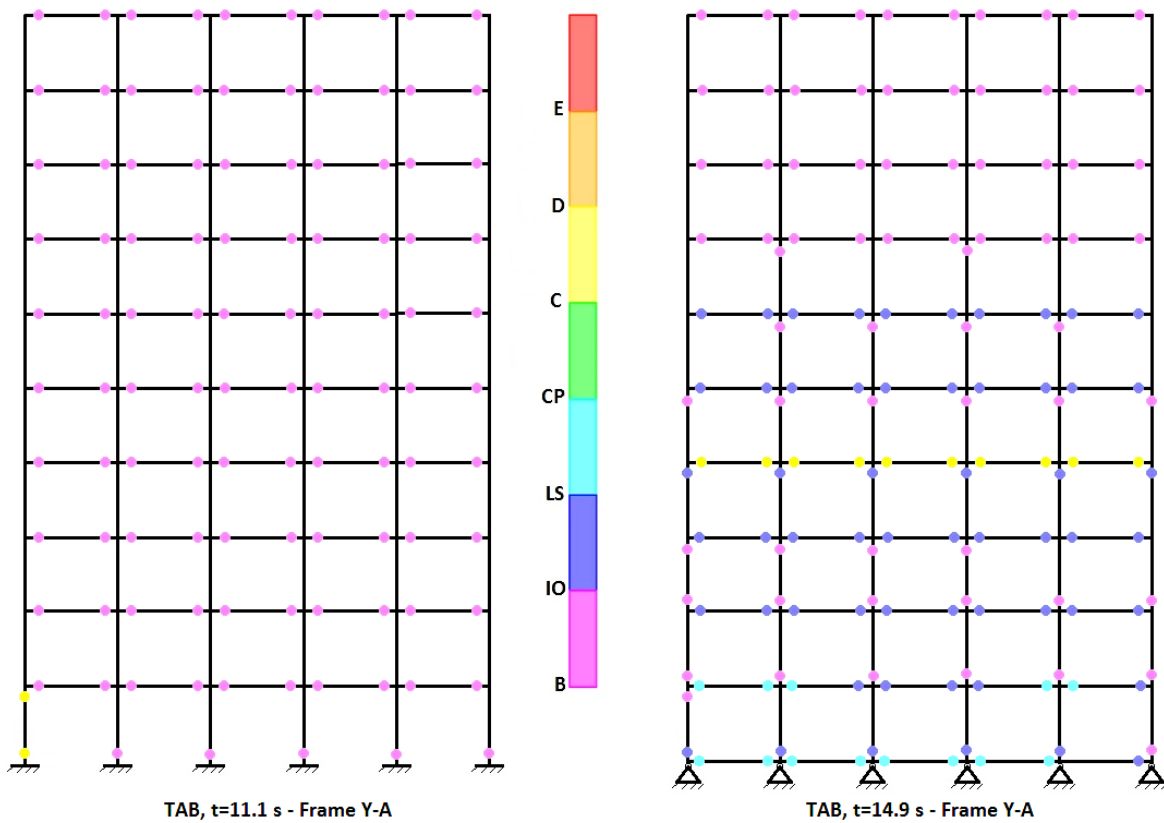


Fig. 15 Seismic performance levels of the 10-story buildings under TAB

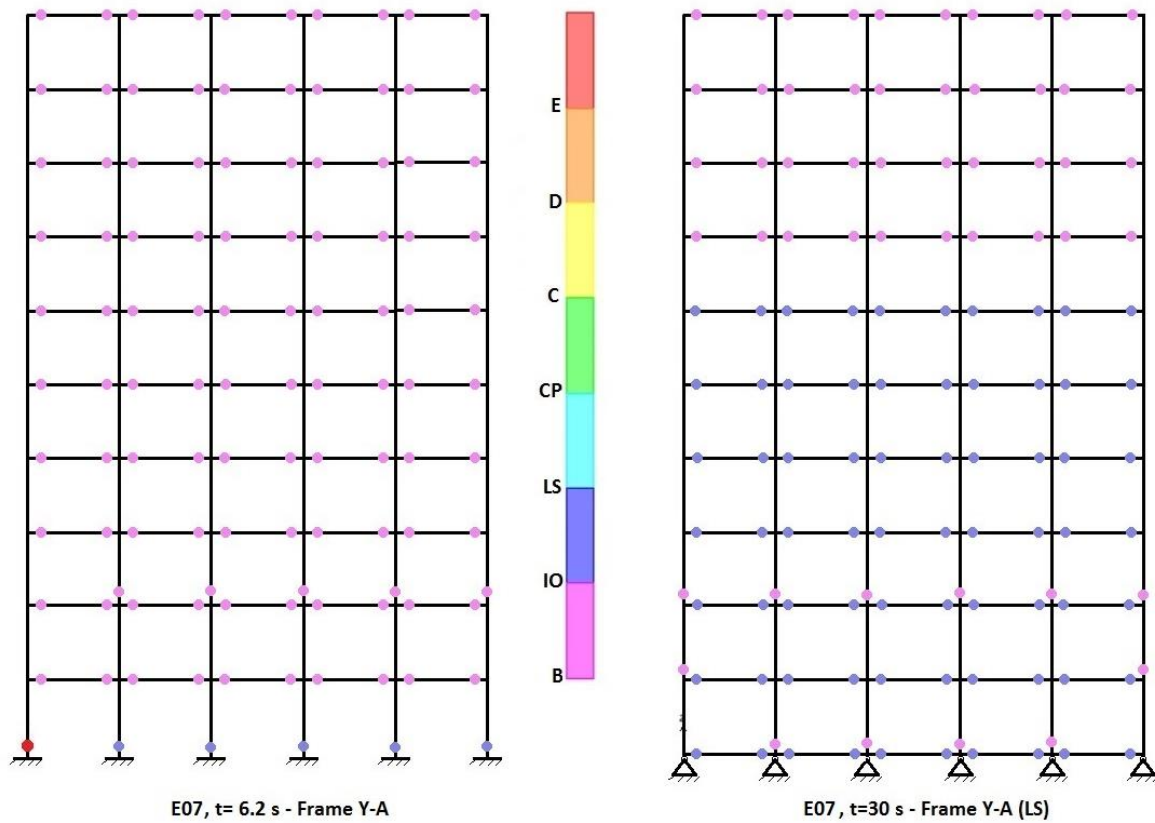


Fig. 16 Seismic performance levels of the 10-story buildings under E07

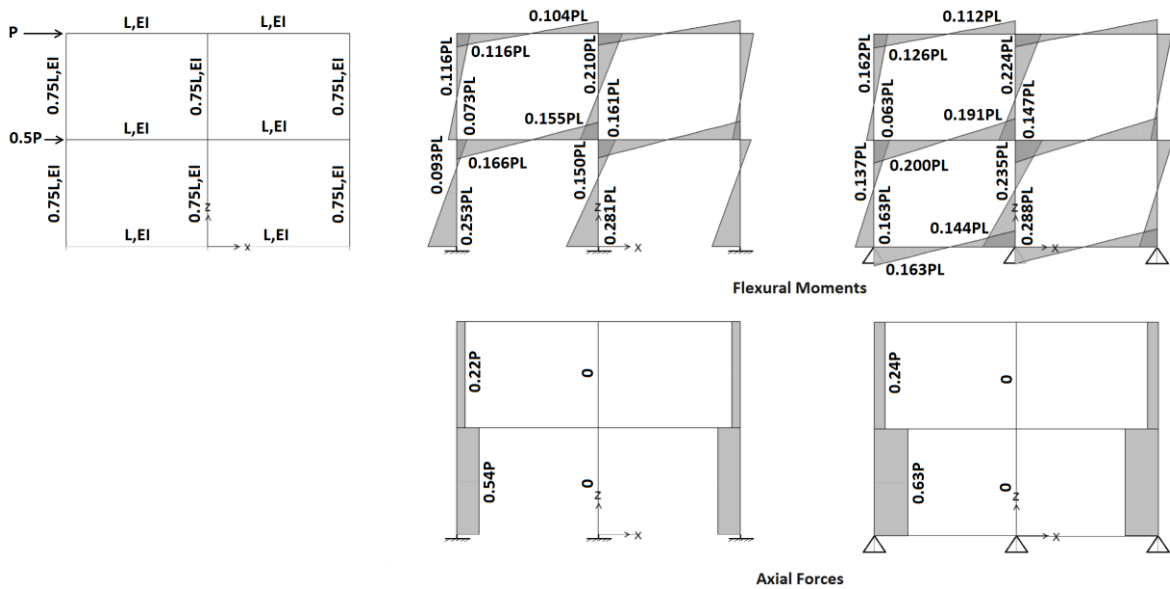


Fig. 17 Structural analysis of a moment frame with different conditions of base connections

more ductility can influence on reducing seismic demands of taller building. Meanwhile, the JOS is a near-fault earthquake with backward-directivity effects. It is substantial to note that the JOS earthquake with backward-directivity effects is similar to a narrow-band excitation. The significant duration of the transversal component of JOS is 27 s. More specifically, equality of the predominant

period of the JOS-TR to the fundamental period of the 5-story buildings causes to dynamic resonance and collapses of the 5-story buildings. While the 10-story buildings remains at IO performance level under the JOS earthquake.

4. Discussion

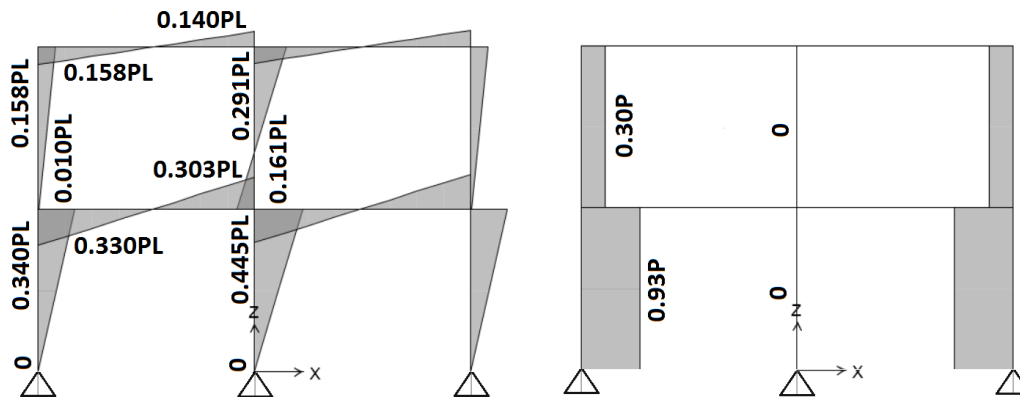


Fig. 18 Structural analysis of a moment frame with fully-hinged connection of the base

According to the aforementioned results, fixed connections of corner columns are the most susceptible locations in the MFFS buildings. As also observed in previous sections, implementing the BLBs as well as hinged connections of the columns to foundation, results in profiting efficiently from the deformation capacity of beams and also decreasing the damages of corner columns. Linear structural analysis of a simple portal, (see Fig. 17) demonstrates the comparison between different types of connections. For the MFHS, the internal moment of the first story corner column is decreased 36% at the base level, while the internal moment of the first story beam is increased 20% compared with the MFFS. Also, the BLBs act similar to the first story beams. Indeed, the moment distribution of the first story frame is changed. It should be noted that, implementation of hinged connection without BLBs (see Fig. 18) leads to high values of axial forces and flexural moments at the ends of first story columns.

Actually, the MFHS buildings which contain BLBs provide the condition of semi-fixity of connections. The sizes of the BLBs are very important. It is so appropriate to construct them with the same size of the first story beams. It is obvious that, supplying more ductility results in more inter-story drift ratios specifically in lower stories; however, employing equipment such as pin-supported rocking walls or dampers may control the drift ratios.

5. Conclusions

The performance of moment frame buildings significantly concerns with the beams manner. If the beams can behave in a desirable ductile manner before collapses of columns, the overall performance of building will be satisfactory. Near-fault strong ground motions have impulsive nature and therefore structural design requires more strength, while providing more ductility causes better patterns of structural damages. The most vulnerable locations of moment frame buildings with fixed supports are the connections of corner columns to the foundation particularly under pulse-type motions. By using hinged connections of columns to the foundation and also BLBs, one can improve the seismic performance of buildings and achieve collapses of beams before columns. Nowadays,

providing hinged or pinned connections in RC structures is available, especially by using precast connections. In this study, the manners of two similar MFFS and MFHS buildings with 5 and 10 stories are assessed under strong earthquakes. Results denote the superiority of performance of the MFHS against the MFFS especially for 10-story building; however, the inter-story drift ratios of lower stories are increased. It is important to point out that the MFHS buildings indicate improved patterns of damages in comparison with the MFFS under strong earthquakes. Remarkable cases are earthquakes such as ABR, TAB, LCN and E07 for the 10-story building and TAB, LCN and JOS for the 5-story building. The key role of the BLB avoids the sudden collapse of corner column. The beams constructed at base level and the first story beams, simultaneously, cause the enhancement of ductility and prevent the collapses of the corner columns. It seems, constructing the BLBs with the same size of the first story beams, yields the best performance. The BLBs can be used as replaceable fuses so as to provide the reparability of buildings.

Acknowledgements

The researchers dedicate this research to the people who lost their lives in near-fault earthquakes such as Tabas 1978 and Bam 2003.

References

- ACI 318 (2014), Building code requirements for structural concrete and commentary, American Concrete Institute; Farmington Hills, MI, USA.
- Alavi, B. and Krawinkler, H. (2001), *Effects of Near-fault Ground Motions on Frame Structures*, John A. Blume Earthquake Engineering Center, California, USA.
- Alavi, B. and Krawinkler, H. (2004), "Strengthening of moment-resisting frame structures against near-fault ground motion effects", *Earthq. Eng. Struct. D.*, **33**(6), 707-722.
- ASCE/SEI 7 (2010), Minimum Design Loads for Buildings and Other Structures, American Society of Civil Engineers, Virginia, USA.
- ASCE/SEI 41 (2013), Seismic Evaluation and Retrofit of Existing Buildings, American Society of Civil Engineers, Virginia, USA.

- Anderson, J.C. and Bertero, V.V. (1987), "Uncertainties in establishing design earthquakes", *J. Struct. Eng.*, **113**(8), 1709-1724.
- BHRC (2005), Iranian Code of Practice for Seismic Resistant Design of Buildings (Standard No. 2800, 4th Edition), Tehran, Iran.
- Bolt, B.A. (1975), "The San Fernando earthquake, 1971. Magnitudes, aftershocks, and fault dynamics", *Bull.*, **196**.
- Champion, C. and Liel, A. (2012), "The effect of near-fault directivity on building seismic collapse risk", *Earthq. Eng. Struct. D.*, **41**(10), 1391-1409.
- Dowrick, D.J. (2009), *Earthquake Resistant Design and Risk Reduction*, John Wiley and Sons, New York, NY, USA.
- Grigorian, C.E. and Grigorian, M. (2015), "Performance control and efficient design of rocking-wall moment frames", *J. Struct. Eng.*, **142**(2), 04015139.
- Hilber, H.M., Hughes, T.J. and Taylor, R.L. (1977), "Improved numerical dissipation for time integration algorithms in structural dynamics", *Earthq. Engrg. Struct. D.*, **5**(3), 283-292.
- Kalkan, E. and Kunnath, S.K. (2006), "Effects of fling step and forward-directivity on seismic response of buildings", *Earthq. Spectra*, **22**(2), 367-390.
- Massumi, A. (2004), "Estimation of response modification factors for RC-MRF structures, emphasizing on the effect of overstrength and redundancy", Ph.D. Dissertation, Tarbiat Modares University, Iran.
- Massumi, A., Mahboubi, B. and Ameri, M.R. (2015), "Seismic response of RC frame structures strengthened by reinforced masonry infill panels", *Earthq. Struct.*, **8**(6), 1435-1452.
- Mazza, F. (2015), "Nonlinear incremental analysis of fire-damaged RC base-isolated structures subjected to near-fault ground motions", *Soil Dyn. Earthq. Eng.*, **77**, 192-202.
- Mazza, F. (2015), "Comparative study of the seismic response of RC framed buildings retrofitted using modern techniques", *Earthq. Struct.*, **9**(1), 29-48.
- Mazza, F. (2017), "Nonlinear response of RC framed buildings retrofitted by different base-isolation systems under horizontal and vertical components of near-fault earthquakes", *Earthq. Struct.*, **12**(1), 135-144.
- Naeim, F. (2001), *The Seismic Design Handbook*, (2nd Edition), Kluwer Academic Publishers, New York, NY, USA.
- Paulay, T. and Priestley, M.J.N. (1992), *Seismic Design of Reinforced Concrete and Masonry Buildings*, John Wiley and Sons, New York, NY, USA.
- Ponzo, F.C., Di Cesare, A., Nigro, D., Vulcano, A., Mazza, F., Dolce, M. and Moroni, C. (2012), "JET-PACS project: dynamic experimental tests and numerical results obtained for a steel frame equipped with hysteretic damped chevron braces", *J. Earthq. Eng.*, **16**(5), 662-685.
- Qu, Z., Wada, A., Motoyui, S., Sakata, H. and Kishiki, S. (2012), "Pin-supported walls for enhancing the seismic performance of building structures", *Earthq. Eng. Struct. D.*, **41**(14), 2075-2091.
- Sehhati, R., Rodriguez-Marek, A., ElGawady, M. and Cofer, W.F. (2011), "Effects of near-fault ground motions and equivalent pulses on multi-story structures", *Eng. Struct.*, **33**(3), 767-779.
- Sorace, S. and Terenzi, G. (2014), "A viable base isolation strategy for the advanced seismic retrofit of an R/C building", *Contemp. Eng. Sci.*, **7**(17-20), 817-834.
- Stewart, J.P., Chiou, S.J., Bray, J.D., Graves, R.W., Somerville, P.G. and Abrahamson, N.A. (2002), "Ground motion evaluation procedures for performance-based design", *Soil Dyn. Earthq. Eng.*, **22**(9), 765-772.
- Takeda, T., Sozen, M.A. and Nielsen, N.N. (1970), "Reinforced concrete response to simulated earthquakes", *J. Struct. Dyn.*, **96**(12), 2557-2573.
- Tasnimi, A.A. and Massumi, A. (2007), *Estimation of Response Modification Factors for RC-MRF Structures*, Building and Housing Research Center (BHRC), Tehran, Iran.
- Van Cao, V. and Ronagh, H.R. (2014), "Correlation between parameters of pulse-type motions and damage of low-rise RC frames", *Earthq. Struct.*, **7**(3), 365-384.
- Zhai, C.H., Zheng, Z., Li, S., Pan, X. and Xie, L.L. (2016), "Seismic response of nonstructural components considering the near-fault pulse-like ground motions", *Earthq. Struct.*, **10**(5), 1213-1232.

CC